Droplet formation by rapid expansion of a liquid

Wm. T. Ashurst*
Combustion Research Facility, Sandia National Laboratories, Livermore, California 94551-0969

Brad Lee Holian
Theoretical Division, Los Alamos National Laboratory, Los Alamos, New Mexico 87545

(Received 12 November 1998)

Molecular dynamics of two- and three-dimensional liquids undergoing a homogeneous adiabatic expansion provides a direct numerical simulation of the atomization process. The Lennard-Jones potential is used with different force cutoff distances; the cluster distributions do not depend strongly on the cutoff parameter. Expansion rates, scaled by the natural molecular time unit (about a picosecond), are investigated from unity down to 0.01; over this range the mean droplet size follows the scaling behavior of an energy balance model which minimizes the sum of kinetic plus surface energy. A second model which equates the elastic stored energy to the surface energy gives better agreement with the simulation results. The simulation results indicate that both the mean and the maximum droplet size have a power-law dependence upon the expansion rate; the exponents are $-2d/3$ (mean) and $-d/2$ (maximum), where d is the dimensionality. The mean does not show a dependence upon the system size, whereas the maximum does increase with system size, and furthermore, its exponent increases with an increase in the force cutoff distance. A mean droplet size of $2.8/\eta^2$, where η is the expansion rate, describes our high-density three-dimensional simulation results, and this relation is also close to experimental results from the free-jet expansion of liquid helium. Thus, one relation spans a cluster size range from one atom to over 40 million atoms. The structure and temperature of the atomic clusters are described. [S1063-651X(99)07406-1]

PACS number(s): 68.10.Cr, 05.70.Ln, 02.70.Ns, 36.40.Qv

I. INTRODUCTION

Atomization of a diesel fuel jet occurs over microsecond time scales (transit time through the orifice) and over submillimeter distances (orifice diameter of a few hundred microns). The breakup of the liquid jet may depend upon cavitation and does involve the creation of a new liquid surface area (formation of droplets from the bulk liquid); neither of these effects is well described by continuum models of fluid dynamics. In order to obtain a direct numerical simulation of the atomization process, the method of molecular dynamics (MD) has been selected. MD assumes classical dynamics and a known potential energy function between atoms, from which one then directly computes the atomic motion. One disadvantage of simulations at the atomic scale is their small size and short time scale. Using the atomic mass, size, and the potential energy well depth, the natural time scale is about one picosecond (the numerical time step is a femtosecond). Thus, an MD simulation at nanoscales (nanometers and nanoseconds) represents a huge task, and simulations at the microscale is a task for future computer hardware. Therefore, at this time we do not simulate the complete fuel jet breakup, but instead use MD to investigate the rapid, homogeneous, adiabatic expansion of a liquid and follow the expansion process into the formation of clusters (i.e., droplets).

The problem configuration in this work is the rapid expansion of a liquid in a system with periodic boundaries in each direction (both two- and three-dimensional systems are examined). From the simulation results we obtain statistical information about the atomic clusters. We start with a Lennard-Jones fluid in equilibrium in the liquid phase (the temperature is near, or above, the critical temperature, and the density is near the triple point value). At time zero of the expansion, every atom is given an impulse proportional to its distance from the origin of the system; the velocity change for the x component is given by ηx, where η is the initial strain rate, and the other components by ηy and ηz (in three dimensions). The system periodic length develops in time like $L(t)=L_0(1+\eta t)$, where L_0 is the initial periodic length, and the periodic boundary velocity is ηL_0 (which remains constant throughout the simulation). The expanding liquid cools down, and temperatures approach the triple point value. As the system expands and doubles and triples its linear extent, there is a rapid change in the number of atomic clusters. At the instant of examination, we define a cluster to be all atoms which are within a selected distance of at least one other atom. The selected distance corresponds to the location of the minimum force, that is, where the force is the most attractive, beyond which the attractive force diminishes to zero. After the periodic length L of the system is more than four times its initial value, further change in the number of clusters is a slow one, so that at some larger expansion ratio, we stop the simulation and gather information about the clusters. The larger clusters are hotter than the smaller ones, and it is expected that they would continue to evaporate until the whole system changes into a gaseous phase (but we do not simulate that aspect of the problem). The initial strain rate (normalized by the molecular unit of time, equal to about one picosecond) has been varied from unity down to 0.0125 in three dimensions and down to 0.05 in two dimensions. The number of atomic clusters depends upon the ini-

*Electronic address: ashurs@ca.sandia.gov

tial strain rate, being larger with larger strain rates. This is reasonable, because a strain rate a little above unity has enough impulse to separate a pair of atoms connected by the Lennard-Jones potential.

Our MD simulations first repeat the work by Holian and Grady [1], in which two-dimensional systems were examined and compared with the energy balance model of Grady [2]. Grady had proposed a model in which the local expansion velocity provides the energy to create a free surface within the bulk liquid, that is, the local kinetic energy from the expansion provides the energy needed to break the bonds between liquid atoms, and thus allow the formation of a liquid surface. As the expansion rate decreases, there will be less energy available unless the domain size increases, and thus lower expansion rates will create larger droplets. Grady's model results in the scaling of size (in number of atoms, μ) versus expansion rate η, as $\mu \sim \eta^{-2d/3}$, where d is the number of space dimensions. Thus, the droplet size will scale as $\eta^{-4/3}$ in two dimensions and as η^{-2} in three dimensions. Holian and Grady did find approximate agreement with this model in their two-dimensional simulation results using a modified Lennard-Jones potential. We extend that work by using longer-range Lennard-Jones potentials. More recently, Toxvaerd [3] has examined two- and three-dimensional systems and compared different procedures for establishing the expansion. Both of these previous studies found a bimodal distribution for the cumulative number of clusters versus the size of the clusters. These distributions depend upon the average cluster size (one exponential term) and the number of monomers (the second exponential term). Our current simulations yield the same bimodal distribution. However, these distributions are also found in the equilibrium fluid structure, and so by themselves do not indicate that fragmentation has occurred [3]. Earlier work by Blink and Hoover [4], in which two-dimensional heated liquids were allowed to expand into a vacuum after the removal of a confining wall, also suggested an agreement with the Grady model.

In the next section we present two continuum models of fragmentation, Grady's and a strain energy one. This is followed by a description of the MD procedure and our two-dimensional results, which is then followed by our three-dimensional results, and a comparison with experimental results.

II. CONTINUUM MODELS OF FRAGMENTATION

We present two continuum models of fragmentation which include estimates of the surface energy based on the atomistic nature of the potential energy at the cluster surface. The first model follows Grady's idea of an equilibrium balance between the expansion kinetic energy and the drop surface energy [2]. The expansion kinetic energy per unit mass is $[d/(d+2)]R^2\eta^2/2$, where R is the radius of the d-dimensional droplet [1]. The surface potential energy per unit mass is $d\gamma r_c/R$, where γ is the surface energy per unit mass and r_c is the thickness of the shell of broken bonds. In terms of the surface to volume ratio, $S=d/R$, the minimization of the sum of these two energies yields a droplet radius of

$$R=\left(\frac{(d+2)r_c\gamma}{\eta^2}\right)^{1/3}. \tag{1}$$

We now must estimate the number of broken bonds at the droplet surface. In the dense state the number of nearest neighbors is equal to $d(d+1)$ and the number of broken bonds may be half of the nearest neighbors or as few as only d neighbors (cleave along a $\langle 111\rangle$ plane in three dimensions and along the line of close-packed atoms in a two-dimensional hexagon crystal). We assume the smaller estimate and let the surface energy term be $\gamma=d\epsilon/2m$. This estimate does not have any temperature or density dependence, and thus it is meant for low-temperature, dense liquids. We also assume that the droplet density is close to the original density and that $r_c\sim\sigma$. This yields the number of atoms in the droplet as $\mu=5.9/\eta^{4/3}$ in two dimensions and $\mu=27/\eta^2$ in three dimensions. These numerical estimates are four and ten times larger than our simulation results to be given below. If we had not minimized the sum of the energies but had just equated them instead, we would obtain an even larger estimate, larger by a factor of $2^{d/3}$.

The second model of fragmentation does not minimize the expansion plus the surface energy but just converts the elastic potential energy Φ_{elastic}, stored up as the system expands from its initial state into surface energy Φ_{surface}, required to break bonds and form free surfaces. Under homogeneous adiabatic expansion at linear strain rate $\eta=d(\epsilon_s)/dt$, condensed matter (either fluid or solid) will fragment when $\Phi_{\text{elastic}}=\Phi_{\text{surface}}$. For simplicity, consider that the material fragments into average-sized cubes in 3D (squares in 2D) of side length L after attaining a critical linear strain in time t of

$$\epsilon_s=\eta t=L/L_0-1, \tag{2}$$

where ϵ_s is the strain and the volumetric strain in d dimensions is $d\epsilon_s$. The stored elastic potential energy in the average fragment of mass M is

$$\Phi_{\text{elastic}}=\tfrac{1}{2}B_0L_0^d(d\epsilon_s)^2, \tag{3}$$

where $B_0=\rho_0c_0^2$ is the bulk modulus, $\rho_0=M/L_0^d$ is the initial density, and c_0 is the bulk-wave speed. The surface potential energy is

$$\Phi_{\text{surface}}=\rho 2dL^{d-1}r_0\gamma, \tag{4}$$

where $\rho=M/L^d$ is the final density of the average fragment with surface area $2dL^{d-1}$, r_0 is the equilibrium bond length (the skin depth of broken bonds at the surface), and $\gamma=d\epsilon/2m$ is the surface energy per unit mass; the bond energy is ϵ and the atomic mass is m. Only half the energy per broken bond at the surface is associated with the given fragment, and there are d missing neighbors at each surface atom. At the critical fragmentation time t, $\Phi_{\text{elastic}}=\Phi_{\text{surface}}$, so that

$$L(\eta c_0t)^2=2r_0\epsilon/m. \tag{5}$$

Notice that the dimensionality factors have vanished. We now suppose that t is the time it takes for a bulk sound wave to cross the distance L of the fragment—a communication

time, or event horizon, between density fluctuations that homogeneously nucleate the fragmentation process; that is, $L = c_0 t$. Hence,

$$L^3 \eta^2 = 2 r_0 \epsilon / m. \tag{6}$$

Consequently, the average fragment size decreases with increasing strain rate by the $-2/3$ power, regardless of dimensionality:

$$L = \eta^{-2/3} (2 r_0 \epsilon / m)^{1/3}. \tag{7}$$

As long as the critical strain to fragmentation is not too large (that is, the strain is small compared to unity so that $\rho \approx \rho_0$), the average fragment mass is then given by

$$M \sim \rho_0 \eta^{-2d/3} (2 r_0 \epsilon / m)^{d/3}. \tag{8}$$

In Lennard-Jones units (σ, ϵ, m), where $r_0 = 2^{1/6}\sigma$, this becomes $M = 2^{7d/18} \rho_0 / \eta^{2d/3}$. In 2D, $\rho_0 = 0.75$ and $M = 1.3/\eta^{4/3}$; in 3D, $\rho_0 = 0.85$ and $M = 1.9/\eta^2$. These elastic energy estimates are much closer to our simulation results: in two dimensions we have agreement with the long-range Lennard-Jones results (force cutoff at 2.5 and 4σ) and in three dimensions the estimate is about 70% of the simulation results. Replacing the cubical shape assumption with a spherical one results in reducing these estimates by a factor of $\pi/4$ in 2D and by $\pi/6$ in 3D, but even these values are in fair agreement with the simulation results. In the second model, the available energy per unit mass is larger than in the kinetic energy-balance model, and with more energy per mass available, there can be more surface atoms created; hence, smaller clusters are formed in the elastic energy-balance model. Two assumptions required in the continuum models are the surface shape and the number of missing bonds that surface atoms have in comparison to the interior atoms. From the cluster simulation results we observe that surface shape, and radius of gyration, change their character over the range of examined expansion rates. Hence, we do not claim that the modeling assumptions used above are to be taken as a detailed picture of actual clusters at specific expansion rates.

III. MD PROCEDURE AND TWO-DIMENSIONAL RESULTS

While our future interest is the atomization in a fuel jet like that used in a diesel engine, we have focused this work on the much simpler problem of a homogeneous expansion of a liquid into a collection of droplets surrounded by its own vapor. Thus we can examine the atomization process in a very simple configuration and obtain guidance about possible behavior in the inhomogeneous fuel jet configuration.

Following Holian and Grady [1], we use periodic boundary conditions in the molecular-dynamics simulations. The use of periodic boundaries reduces the dependence upon the number of atoms used in the simulation. A simulation of a periodic system in equilibrium maintains all the atomic coordinates within the range of $(0,L)$ by adding or subtracting the system edge length L whenever an atom coordinate exceeds this range. To simulate an expanding system, the atomic velocity must also be adjusted when the atom crosses a periodic boundary. As in the previous work, we define the linear expansion rate as η. The expansion rate η is constant throughout a particular simulation and the periodic domain edge length grows like $L(t) = L_0(1 + \eta t)$. At the start of the expansion process—time zero—the velocity of each atom is given an impulse equal to its distance from the system origin. Thus, the atom velocity at that instant is enhanced by ηx, ηy, and in three dimensions by ηz. The periodic boundary velocity is thus equal to ηL_0 and remains constant throughout the simulation. The boundary velocity at the origin is considered to be zero, and so the jump velocity across the system equals ηL_0 in each coordinate direction. Hence, when the atomic location is adjusted because of a boundary crossing, its velocity corresponding to that coordinate direction is also adjusted by adding or subtracting ηL_0. We have only used systems with equal values of η and L_0 for all coordinate directions. (Toxvaerd [3] has investigated the use of this initial impulse method by comparing with systems in which the boundary confinement is just moved at a fixed rate. When the expansion rate is small compared to the time required for sound waves to communicate from the boundary to the interior of the system, he finds that the initial impulse method is an efficient way to achieve a homogeneous expansion.)

We use the pairwise-additive Lennard-Jones potential as a representative interaction between molecules. While not an exact potential of any material, it does exhibit the transition between the liquid and gaseous phases, which is the important feature in the atomization process. Thus, droplet surface tension will be an outcome of the simulations. The Lennard-Jones (LJ) potential energy is

$$\phi(r) = 4\epsilon[(\sigma/r)^{12} - (\sigma/r)^6]. \tag{9}$$

The value of the minimum energy is $-\epsilon$, which occurs at $r_0 = 2^{1/6}\sigma$. This is also the location where the force changes from repulsive to attractive. The force between two atoms is given by the negative gradient of their potential energy, $\mathbf{f} = -\boldsymbol{\nabla}\phi(r)$. The atomic positions are advanced using the Stoermer-Verlet [5] time-centered finite-difference equation

$$\mathbf{r}(t + \delta t) = 2\mathbf{r}(t) - \mathbf{r}(t - \delta t) + \mathbf{f}(t)\,\delta t^2/m + O(\delta t^4), \tag{10}$$

and the time-centered velocity is found from $[\mathbf{r}(t + \delta t) - \mathbf{r}(t - \delta t)]/(2\,\delta t)$; typical time-step values are $\delta t = 0.01 t_0$ and $0.004 t_0$, where $t_0 = \sigma\sqrt{m/\epsilon}$ is the LJ unit of time. The harmonic frequency associated with the force at the location r_0 is the fundamental frequency obtained from $m\omega_0^2 r_0^2 = r_0^2 \phi''(r_0) = 72\epsilon$. This frequency is $\omega_0 t_0 = 7.56$. The potential inflection point is the minimum force location, beyond which the attractive force diminishes with increasing distance. The minimum force occurs at $(26/7)^{1/6}\sigma \sim 1.24\sigma \sim 1.10 r_0$. The force interaction is truncated at a finite distance in order to reduce the computational work in calculating the atomic motion. A popular force cutoff distance is 2.5σ. In addition to truncating the force interaction, the potential is also shifted so that it is exactly zero beyond the cutoff distance. This truncation and shifting affects the phase diagram of the system. For example, in three dimensions, the full Lennard-Jones potential has a critical point value that is estimated to be $T = 1.316\epsilon/k$, whereas truncation of the potential to 2.5σ reduces the critical temperature to 1.085 (see

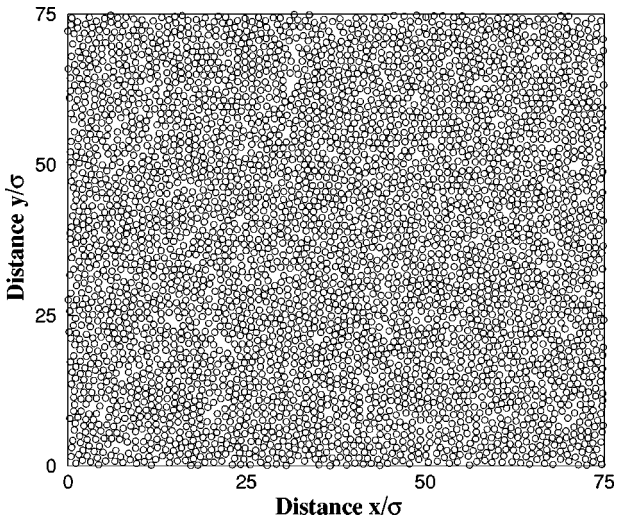

FIG. 1. An initial two-dimensional liquid configuration with a reduced density of 0.75 and a reduced temperature of 0.6; Lennard-Jones potential with a force cutoff at 2σ.

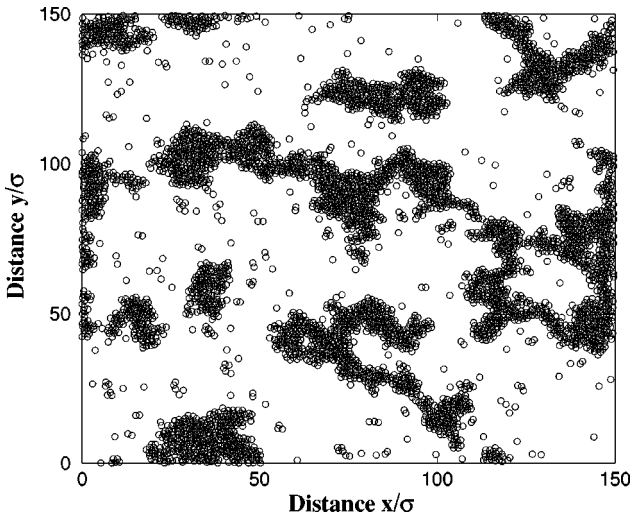

FIG. 2. Clusters formed by expanding in 2D at the rate $\eta = 0.01$ until the domain size has doubled.

Smit [6] and Johnson *et al.* [7]). In two dimensions, the full Lennard-Jones potential has a critical density of 0.355 and a critical temperature of 0.515, but when the potential is truncated at 2.5σ and the potential is shifted to be zero at the cutoff, then the critical temperature is reduced to 0.459 while the density does not change (Smit and Frenkel [8]). The estimated triple point temperature is 0.41 (2D) and 0.69 (3D); units of ϵ/k will be used in the following.

Holian and Grady not only truncated the Lennard-Jones potential, but they also changed its shape between the minimum force location and a cutoff location by using a cubic spline function. In this way they impose the condition that the potential goes smoothly to zero at the cutoff distance, 1.74σ [see Eq. (A5) in Holian and Ravelo [9]]. The effect of this modification upon the phase diagram is not known. We compare simulations using their potential with simulations using the LJ potential truncated at 2, 2.5, and 4σ; we do find some small differences in the cluster behavior.

We now present our two-dimensional results. Using the same Lennard-Jones/cubic potential (LJ/cubic) as Holian and Grady, as well as the same number of atoms ($N=4200$), we examine the range of linear strain rate from 0.0535 to 0.856, using a time step of $0.01t_0$. A snapshot of the initial liquid configuration is given in Fig. 1 and the resulting clusters formed by different expansion rates are shown in Figs. 2–4 (our Fig. 3 compares well with Fig. 4 in Holian and Grady; they give the volume strain rate, which is twice the linear value in 2D). The cluster distributions are determined when the bulk density equals 0.175 (a linear expansion of 2.07 from the initial density of 0.75). A cluster is composed of all those atoms which are connected to at least one other atom by a prescribed distance, namely, a bond length corresponding to the minimum force distance, $r_c = 1.24\sigma$. The selection of this distance can be considered to be following the guidance of the Lindemann melting law; that is, when the root-mean-square displacement of the atomic motion exceeds a small distance compared to the nearest-neighbor separation, a solid is likely to melt [10]. (We note here that use of the force cutoff distance to determine the clusters yields results which vary with the cutoff distance, whereas using the minimum force distance yields results which have little dependence upon the cutoff distance.)

Holian and Grady obtained distributions of cluster size which are bimodal exponentials:

$$C(n) = \int_n^\infty dn' S(n') = N_m e^{-n} + N_c e^{-n/\mu}, \qquad (11)$$

where n is the number of atoms in the cluster, $C(n)$ is the cumulative number of clusters of size greater than n atoms, $S(n)$ is the spectral distribution, or number of clusters of size n, N_m is the number of monomers, N_c is the number of clusters, and μ is the average number of atoms in a cluster. Excluding the monomers from consideration, then the straightforward determination of the average number of atoms in the clusters is given by $\mu = (N - N_m)/N_c$. This average number includes the contributions from the small clusters, that is, the dimers, trimers, and so forth, which are also determined by the monomer distribution. Therefore, Holian and Grady determine the average cluster size μ by examin-

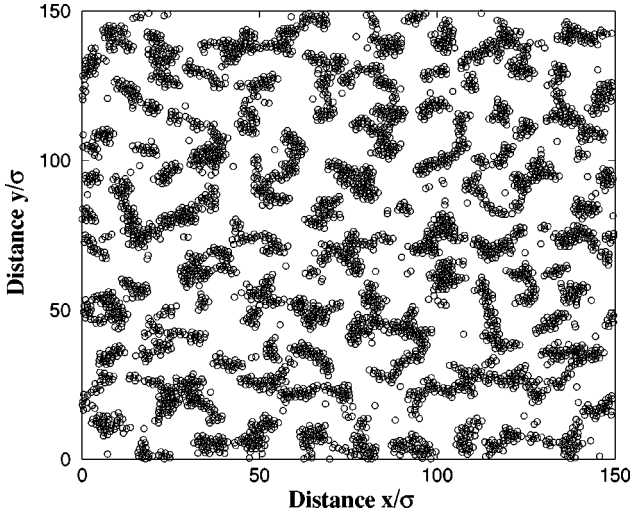

FIG. 3. Clusters formed by expanding in 2D at the rate $\eta = 0.1$ until the domain size has doubled.

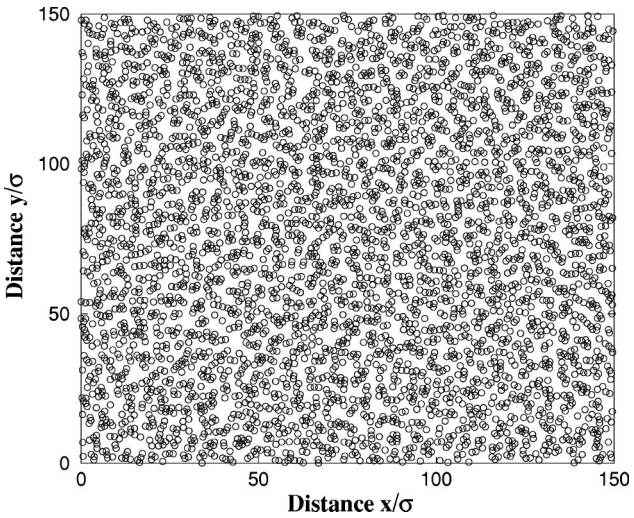

FIG. 4. Clusters formed by expanding in 2D at the rate $\eta=1$ until the domain size has doubled.

ing the distribution and selecting a value of μ which allows a match with the results in the region beyond the influence of the monomer distribution. We use

$$C(n)=N_m e^{-n}+\frac{N-N_m}{\mu}e^{-n/\mu}, \tag{12}$$

where the number of atoms that are in clusters is $N-N_m$, and μ is the average cluster size as determined by fitting the distribution. Typical cumulative distributions are given in Fig. 5.

Of interest is the dependence of μ upon the potential, the dimensionality, and the amount of expansion. From the Grady model of converting expansion kinetic energy into surface energy, we have the concept that the average cluster size will have a power-law dependence upon the expansion rate, namely that in d dimensions the average cluster size μ will be given by $\mu\propto\eta^{-2d/3}$. We also examine the maximum cluster size and its dependence upon the expansion rate.

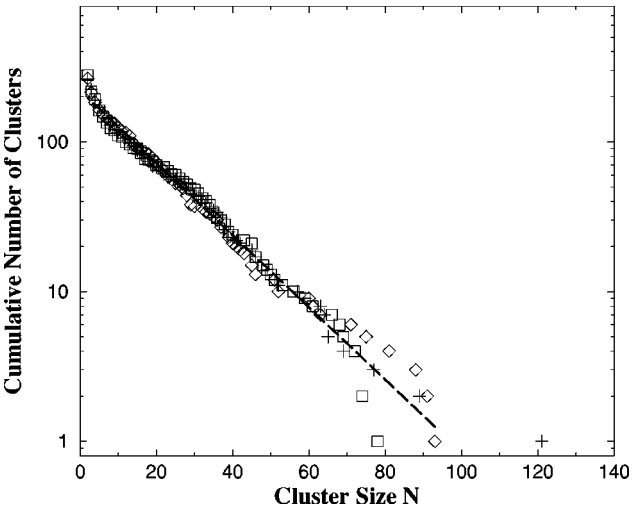

FIG. 5. 2D cluster distribution with expansion rate $\eta=0.107$, using the LJ/cubic potential. Three realizations are shown along with the estimated fit to the mean result (dashed line). Notice that the maximum cluster size ranges from 80 to 120 atoms.

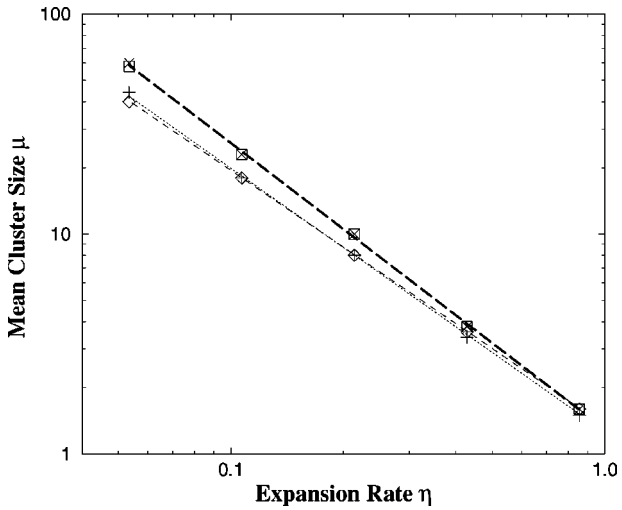

FIG. 6. 2D mean cluster size, μ dependence upon expansion rate, η, and upon the potential: LJ/cubic ($\diamond$), LJ truncated at 2σ ($+$), at 2.5σ ($\square$) and at 4σ ($\times$).

From the cumulative distribution we estimate the maximum cluster size by setting $C(n_{\max})=1$, and assuming that the monomer contribution is zero, we have an approximation for the maximum cluster size as

$$n_{\max}=\mu\ln[(N-N_m)/\mu]\approx\mu\ln(N/\mu), \tag{13}$$

where in the last approximation the monomers are ignored and N_f is replaced by N.

We now describe the two-dimensional results using different force laws and different force cutoff distances. The initial equilibrium state is created from $N=4200$ atoms on a regular lattice of density 0.75 (near the triple point value) with randomly drawn velocity components; enforcement of the desired temperature of 0.6 (above the critical temperature) is achieved by velocity rescaling during an equilibration time of $10t_0$ prior to expansion. Different realizations are created by changing the random number seed for the velocity selection. Three realizations have been used for most conditions (and checked with five realizations at low expansion rate).

We find that the average cluster size does change with the force cutoff distance; see Fig. 6. The shortest cutoff, the LJ/cubic with $r_{\rm cut}=1.74\sigma$, yields the lowest exponent, $\mu=1.35/\eta^{1.16}$ (indicated by the short dashed line). The Lennard-Jones potential with $r_{\rm cut}=2\sigma$ gives $\mu=1.26/\eta^{1.2}$ (dotted line), while $r_{\rm cut}=2.5\sigma$ gives $\mu=1.3/\eta^{1.3}$, but a further increase in $r_{\rm cut}$ to 4σ does not cause a further change (bold dashed line). The maximum cluster size, as observed in five realizations using the LJ potential truncated at 2.5σ, can be approximated by $10/\eta$, but as discussed below, we suspect that the maximum cluster size is restricted by the finite system size when the expansion rate is small.

Based on these 4200-atom two-dimensional results, we conclude that the range of the force has a small effect, namely, increasing the range also increases the exponent of average cluster-size dependence upon the expansion rate. The two larger cutoffs with the LJ potential produce results which agree with the Grady model of cluster-size variation with expansion rate, namely that the average cluster size will

have a dependence like $\eta^{-4/3}$ in two dimensions. The truncation of force in the Lennard-Jones cases causes a finite jump in the force at the cutoff location. This force jump does not occur in the LJ/cubic model, and since its results agree with the trend of the LJ results, we conclude that the force jump is not a serious blemish in the dynamics.

IV. THREE-DIMENSIONAL MD CLUSTER RESULTS

Three system sizes have been used in three dimensions: $N=4000$, 32 000, and 256 000 atoms; they will be denoted as 4, 32, and 256 K. In all systems the maximum expansion rate is $\eta=2$ and the minimum values are 0.125 (4 K), 0.0125 (32 K), and 0.05 (256 K). Computational cost restricted the minimum expansion rate in the largest system while the creation of too few clusters restricted the minimum rate in the smaller systems. Five realizations were created at each expansion rate value. Most of the simulations had an initial density of 0.85 (triple point) and an initial temperature of 1.4 (the critical temperature is estimated to be 1.085 when the potential is truncated at 2.5σ and the potential is also shifted to be exactly zero beyond the force cutoff; see Smit [6]). A few simulations have also been made with a force cutoff of 4σ, which has a critical temperature of 1.246. The full potential critical temperature is 1.316, and the estimated triple point temperature is 0.69 [7]. The time step is $0.004t_0$.

We observe that the expansion changes the average potential energy, with diminishing change as the expansion rate becomes small. The initial liquid state has a potential energy which is negative (from -5.24 at $T=0.7$ to -4.28 at $T=1.7$), reflecting the many neighbors which are located near each atom. The expansion process creates fragments, and the atoms near the surface of a fragment will have a potential energy higher than the initial liquid-state value, because these surface atoms now have fewer neighbors. To describe the change in the average potential energy, we compare the energy when the domain size has expanded to $3L_0$, to its initial value, when the domain size is L_0. We find that systems with initial temperatures of 0.7, 1.4, and 1.7 have almost the same reduced potential energy change with respect to the expansion rate, namely $(\phi_{L_0}-\phi_{3L_0})/\phi_{L_0}\approx 0.8\eta^{1/3}$.

From these simulations the cluster information was obtained at integer increments of the initial domain size, L_0. Detailed information was studied at domain sizes of $3L_0$, $6L_0$, and $13L_0$. At $2L_0$ with low expansion rate, the largest cluster was essentially equal to the system size. Beyond $3L_0$, the number of clusters has reached a quasisteady value. At large expansion rate, about two-thirds of the atoms are monomers, and this value is almost constant over the expansion duration. On the other hand, at low expansion rate, the number of monomers grows with the increasing domain size at a rate independent of the strain rate. At $6L_0$ the number of monomers is 21% of the total number of atoms; at $13L_0$, the fraction of atoms that are monomers has grown to about one-third. As discussed by Toxvaerd [3], at very small expansion rates, the adiabatic expansion becomes a reversible one, and the structure of the system is that of the equilibrium state. However, we note that an expansion of a two-phase system would produce monomers at a rate proportional to the cube of domain length, which is far larger than what we observe in our simulations.

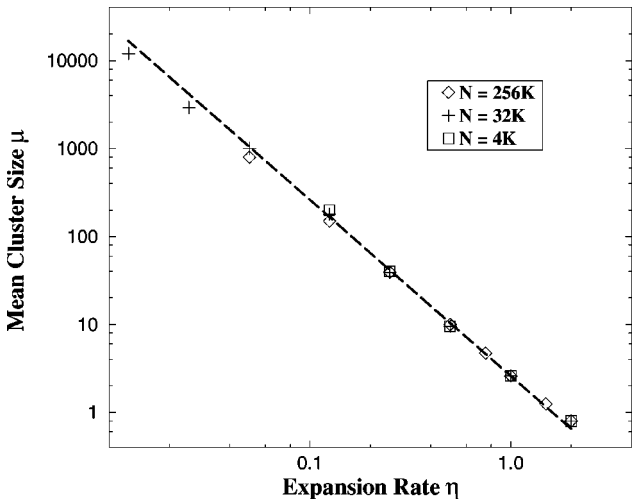

FIG. 7. The mean cluster size in 3D increases with decreasing expansion rate; the dashed line equals $2.6/\eta^2$; these results are based on five run averages, domain size is $6L_0$, and the initial density is 0.85.

The five realizations at each expansion rate are pooled together to obtain a mean and standard deviation of the number of clusters at each possible cluster size. In each realization, linear interpolation is used between the actual clusters of that realization to generate information at integer values of cluster size. To determine the mean cluster size μ at a given expansion rate, a plot of the mean cumulative cluster distribution is made along with the function $be^{-n/\mu}$. The values of b and μ are adjusted to match the distribution in the cluster size region just beyond the tail of the obvious monomer distribution. Note that extension of these fits on the linear-log plot does not always coincide with the observed mean value of the maximum cluster size.

Figure 7 presents the mean cluster size determined from the graphical procedure described above; there is no obvious dependence upon the system size. The 21 values in Fig. 7 have a relative rms error of 0.17 with respect to $\mu=2.6/\eta^2$ (dashed line). The initial temperature of these results is 1.4, and to determine a possible temperature influence, simulations with initial temperatures of 1.7 and 0.7 were also generated using a 32 K system. Single run realizations produced mean cluster sizes that are in agreement with those shown in Fig. 7. Because the mean cluster size increases with decreasing expansion rate, we suspect that the lower expansion rates produce results which are less reliable than those produced with the higher rates (within a system of the same size).

Using the 32 K system size, other initial densities were examined, with $0.025\leqslant\eta\leqslant 1$. Simulations with an initial density of 0.94 are described by $\mu=2.8/\eta^2$ (with relative error of 0.07). Thus, as in the continuum models, the prefactors appear to have a linear density dependence. With lower initial densities of 0.76 and 0.68, the mean cluster size is given by $\mu=2.2/\eta^{1.87}$ and by $2.0/\eta^{1.71}$. Using an exponent of 2 with these two densities produces a much larger error than that observed in the two higher density cases. We find that these low-density cases are sensitive to the force cutoff value. By changing the cutoff from 2.5σ to 4σ, the 0.68 density result changes from $2.0/\eta^{1.71}$ to $\mu=2.2/\eta^{1.85}$, an increase of 10% in both the exponent and the prefactor. Thus,

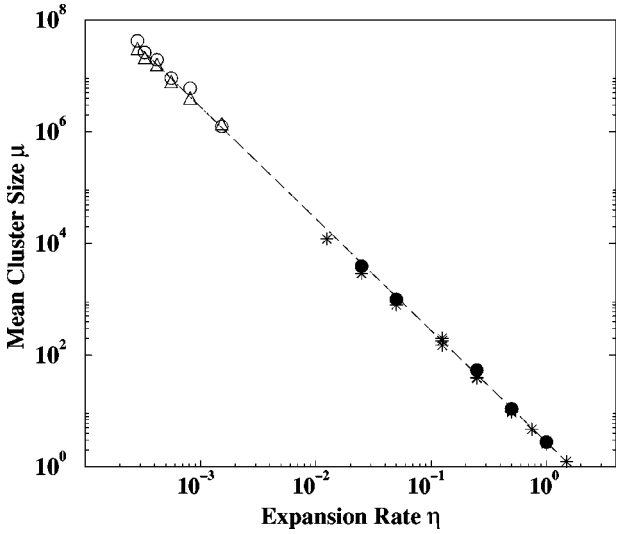

FIG. 8. Droplet mean size from liquid helium free-jet experiments (circles and triangles) and from 3D MD simulations: initial density of 0.85 (stars) and 0.94 (filled circles) vs expansion rate η; the dashed line is $\mu = 2.8/\eta^2$.

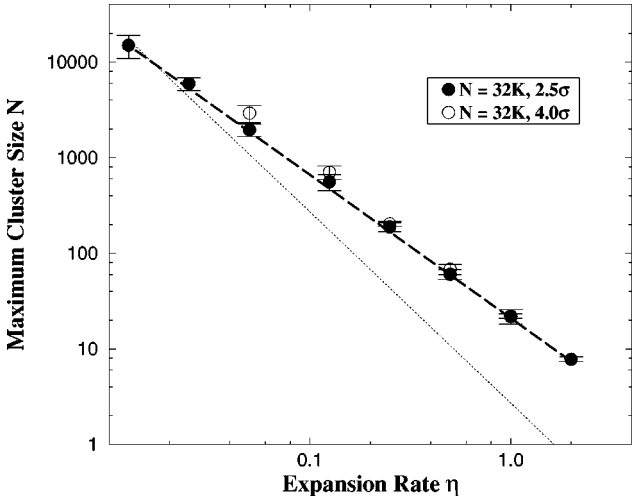

FIG. 9. The 3D maximum cluster-size dependence upon the force cutoff distance. 32 K results with a cutoff of 2.5σ are described by $22/\eta^{1.5}$ (dashed line), while a larger cutoff of 4σ produces results with a larger exponent, $22/\eta^{1.64}$ (circles). These results are based on five run averages. Error bars correspond to one standard deviation. The dotted line is the mean cluster size from Fig. 7.

with even larger cutoff values (as suggested by Mecke *et al.* [11]), these low-density cases may also approach more closely the expected quadratic dependence upon strain rate, but, due to the increased computational cost, we have not pursued this issue. At high density, however, a similar increase in the cutoff distance, with an initial density of 0.85, produces no change in the mean cluster size from that given above. We conclude that in order to observe the exponent that is predicted by the continuum models, the lower initial densities require a larger force cutoff value than that needed by the higher initial densities. The numerical prefactor constants predicted by the continuum models, with an initial density of 0.85, are 27 (kinetic surface) versus 1.9 (elastic surface with cubical shapes).

The elastic-surface model and the MD results also agree with experimental information obtained by Knuth and Henne. Knuth and Henne [12] have used free-jet expansion of liquid helium to create liquid fragmentation, and from their data they have estimated the mean cluster size as a function of the jet diameter d^* and the jet sound speed a^*; these two parameters define a strain rate. Using the Grady model (kinetic surface), Knuth and Henne determine the mean cluster size as $\mu = (80\pi/3)\Phi$, where $\Phi = \gamma(d^*/a^*)^2$ is their dimensionless fragmentation parameter and γ is the surface tension per unit mass. However, by comparison with their data, they note that this numerical prefactor is almost 30 times too large; a prefactor of 3 describes their data over the range of one million to 40 million atoms. This approximate expression is also consistent with our MD results based on systems with only a quarter of a million atoms in which the mean cluster size is 10^4 and less. Using $3\Phi = \mu = 2.8/\eta^2$, we compare the two results in Fig. 8. A strong caution must be given with regard to this comparison: the flow-induced strain rates created in the jet are more complex than the uniform expansion rates in the MD simulations; indeed, it is possible that additional factors as large as 3 could enter into the comparison given above. To illustrate possible effects of different volume strain-rate compositions, we have expanded a 32 K system with η in two directions and with no expansion in the third direction. Based on volume strain rate, the expected mean cluster size would be $\mu = 2.6/(2\eta/3)^2 = 5.85/\eta^2$ (the density is 0.85 and the force cutoff is 2.5σ); the observed result is a numerical prefactor which is 20% larger than the expected one.

While the mean cluster size does not show a dependence upon the system size, this is not true for the behavior of the maximum cluster size; we obtain larger values in larger systems. The results, with a force cutoff of 2.5σ, appear to exhibit a size dependence that can be described by $22/\eta^{3/2}$ for the 32 K results, with numerical prefactors of 18.5 for the 4 K and 25.2 for the 256 K results. This exponent value is dependent upon the force cutoff distance. Figure 9 presents 32 K results using a cutoff of 2.5σ and 4σ, with an initial density of 0.85. We see that the maximum cluster size is clearly larger at low expansion rates with the use of a larger force cutoff.

From the cumulative distribution of clusters, it is possible to estimate the maximum cluster size, using Eq. (13); this estimate leads to $n_{\max} \approx \mu \ln(N/\mu)$. This logarithmic dependence on N yields a factor of 4 increase between the 4 and the 256 K results, whereas the actual increase is a much lower ratio of 1.36. Thus, while the cumulative cluster distribution does offer a guide to the maximum cluster-size dependence upon the expansion rate, the distribution estimate vastly overpredicts the magnitude of the N dependence. The apparent crossover of the mean cluster size and the maximum size (dotted and dashed lines in Fig. 9) is probably an artifact of the finite-system size, as well as the effect of the finite force range upon the maximum cluster size.

In Appendix A, we describe the observed cluster temperatures. The results show that the smaller clusters are colder, while the larger ones are hotter. In Appendix B, we discuss cluster shapes and show that clusters become more spherical at lower strain rates. In Appendix C, we discuss the bonding in clusters and show that the larger clusters at low expansion rates exhibit densities near the triple point value.

V. CONCLUSIONS

A liquid will flow under the action of an applied force, and a liquid cannot sustain a tensile load for a long time. With these properties, how does a liquid fracture? We have used molecular-dynamics simulations to study the atomization process when a liquid is rapidly expanded into the gaseous-phase region. We find that as long as modifications to the interatomic pair potential are restricted to the attractive region beyond the inflection point, there is minimal effect on the nonequilibrium process of fragmentation in the dense liquid.

Under homogeneous expansion, with linear expansion rates η ranging over two orders of magnitude, we show that the average cluster size is given by $\mu = \text{const}/\eta^p$, where the exponent $p = 2d/3$ in d dimensions appears to agree with two simple continuum models: the first model, developed by Grady, minimizes the sum of expansion kinetic energy and surface energy, and overestimates our simulation results; the second model equates the stored elastic energy to the surface energy, and gives more reasonable agreement. In both cases, expansion energy goes into creating new liquid surface, so that the average size of the clusters decreases when more energy is available.

We observe that the cluster behavior is quasisteady while the expanding domain in the simulation grows from 3 to 10 times its initial linear extent. The cumulative number of clusters is well described by a bimodal distribution (sum of two exponentials). Starting with the largest clusters, the first mode governs the average large-cluster size, while the second governs the number of monomers. The distributions are based on cluster mass and number of atoms; at low expansion rates, a distribution based on cluster diameter (cube root of mass) appears to provide the same mean cluster size. We have studied the cluster temperature, and find that it increases gradually with cluster size. At sufficiently low expansion rates, we note that the average cluster size begins to approach the maximum size; that is, the distribution describes large monodisperse droplets surrounded by vapor, which could be symptomatic of the beginnings of system-size limitations to our MD simulations. We have not explored below this apparent limit of very slow expansion rates, but note that the MD results and liquid helium results are both well described by an average cluster size of $2.8/\eta^2$; the helium results involves clusters which are a hundred times larger than any of the MD clusters.

ACKNOWLEDGMENTS

This work was supported at Sandia Livermore by the U.S. Department of Energy (DOE), through the Office of Basic Energy Sciences, Division of Chemical Sciences, and at Los Alamos by the U.S. DOE, through the LDRD CD Thrust ''Multiscale Science.'' We acknowledge helpful discussions with Bill Hoover, Alan Kerstein, Eldon Knuth, and Dennis Grady. Permission to reproduce the Knuth and Henne data is appreciated.

APPENDIX A: CLUSTER TEMPERATURE

The translational temperature can be based on either the atom velocities with respect to the mean expansion motion or, for clusters bigger than monomers, relative to the mean motion of their cluster (the resulting temperatures differ by a few percent). The temperature defined by all the atoms with respect to the expansion motion ranges from 0.2 (at $6L_0$, $\eta = 2$) to 0.5 ($\eta = 0.25$); the temperature of the monomers is about 60% of these values (while the fraction of monomers varies from $0.6N$ down to $0.2N$ over this η range). Thus, the monomers do not exhibit a very large velocity variation about the mean expansion motion; they are quite cold. The atomic velocities (u,v,w) with respect to their cluster mean velocity are used to define the cluster translational temperature using $3(n-1)kT = m\Sigma(u_i^2 + v_i^2 + w_i^2)$, where the summation is over the n atoms in the cluster, and the factor $n-1$ reflects that the velocities are with respect to the mean mass motion of the cluster. If there is more than one cluster of a given size in the realization, the temperatures are averaged. Then these cluster temperatures are gathered over the five realizations at that expansion rate in order to determine a mean cluster temperature and an estimate of its standard deviation (see Fig. 10, diamond symbols with error bars). Because there are very few large clusters, the deviation of the large cluster temperature is greater than that of the small cluster temperature, about 5% compared to 1%.

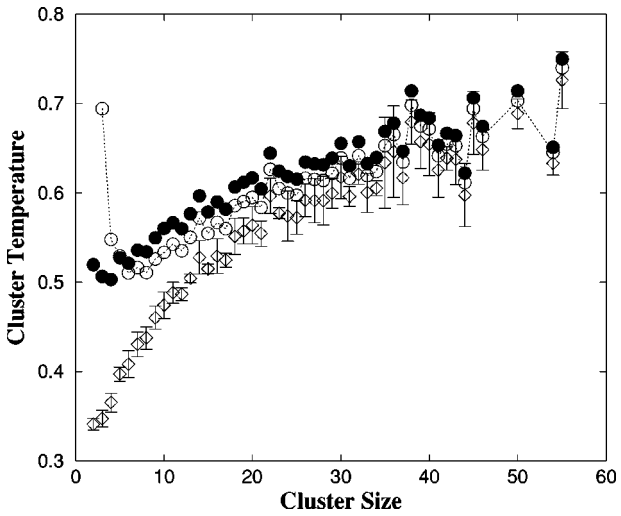

FIG. 10. 3D cluster temperature in 32 K system at $\eta = 0.5$; translational temperature (diamond symbols with error bars which denote one standard deviation based on five realizations), translational plus rotational temperature (filled circles), and a temperature estimate based on restricting six degrees of freedom (open circles connected by a dashed line).

The largest clusters have temperatures near the triple point value (estimated to be 0.69) and the smaller clusters are much colder, approaching values near 0.35. However, the smaller clusters have a significant amount of rotational energy. We define a rotational temperature as $T_r = \mathbf{L}\cdot\mathbf{L}/(knI)$, where $\mathbf{L}$ is the angular momentum and I is the moment of inertia of a cluster with n atoms. Figure 10 presents the sum of the rotational and translational temperature (filled circles) along with the estimate given by restricting six degrees of freedom in the cluster: $3(n-2)kT_a = m\Sigma(u_i^2 + v_i^2 + w_i^2)$. The values of T_a are shown by circles connected with a dashed line in Fig. 10. The estimate T_a is too large when the cluster has fewer than five atoms, and too small for larger clusters. Since the clusters are defined by

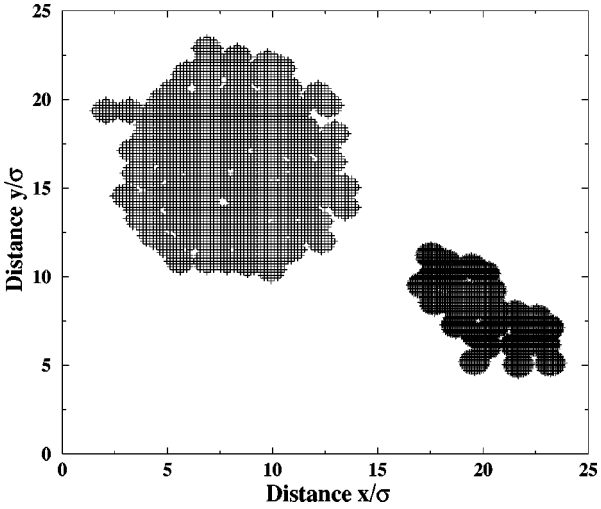

FIG. 11. Projected view of two clusters. The larger one has 535 atoms and was formed with an expansion rate of 0.125, while the smaller one, created by $\eta=0.5$, has only 56 atoms.

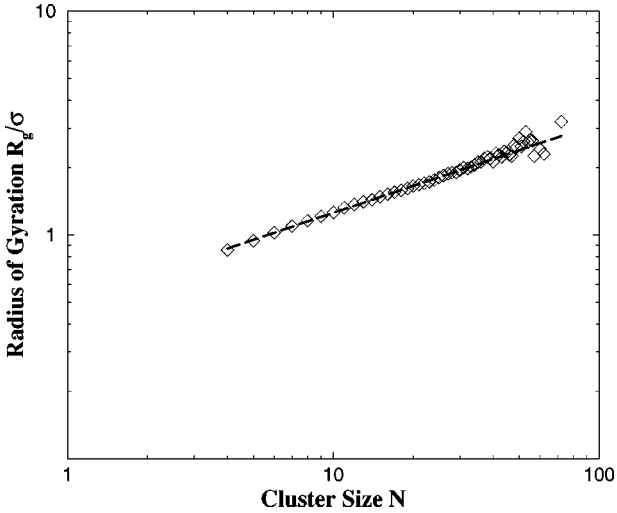

FIG. 12. Radius of gyration versus cluster size has a fractal character when the expansion rate is larger than 0.125; here $\eta=0.5$ and the dashed line indicates a fractal dimension of 2.5; results from 32 K system size.

their geometric arrangement at the instant of examination, and not over a finite time interval, then the overprediction for the smallest clusters may reflect cases in which the atoms are undergoing a collision process rather than being bound together with a negative total energy. Thus, on the whole, restricting six degrees of freedom offers a good estimate of the cluster temperature. In the two-dimensional expansion work of Blink and Hoover [4], the rotational temperature was examined and found to be of insignificant value.

Using a 32 K system, we examine the cluster temperature in low-density equilibrium systems. A density of 0.0315, corresponding to a domain size of $3L_0$ in an expanding simulation, was used at two different temperatures: 0.5 and 1.4. The initial atom locations are on an fcc lattice with random velocities drawn from a Maxwell-Boltzmann distribution based on the desired temperature. The mean temperature is enforced during the simulation by rescaling all the atom velocities at each time step, over a time period of $200t_0$. In the colder simulation the atoms condense into clusters during the simulation and the average potential energy continues to decrease with increasing time. We pick a time when the maximum cluster size is similar to that of an expanding simulation at a low expansion rate. The variation of cluster temperature is similar to the expanding system: the larger clusters are hotter than the smaller ones. In the equilibrium simulation with a temperature above the critical point, the average potential energy reaches a constant value early in the simulation, and the number of clusters also reaches a constant value. The maximum cluster size is much smaller than the cold case (8 compared to 63), and these small clusters are colder than the mean temperature. In this warm system, a cluster can maintain its structure if it has low energy (colder than the mean), while in the cold system (below the triple point) the rare larger clusters have more energy than average.

APPENDIX B: CLUSTER SHAPES

Figure 11 presents a projected view of two clusters: one appears circular and the other elongated. The circular one was created with a low expansion rate ($\eta=0.125$) and the smaller, elongated cluster by a large rate ($\eta=0.5$). These images were formed by filling in cells on a grid if they are within a certain distance of any atom center in the projected view. The selected distance is 0.62σ (half of the cluster-defining distance) and the cell sizes are 0.16 ($\eta=0.125$) and 0.08σ. In addition to these projected views, we also examine the cluster moments of inertia and compare with other studies of equilibrium clusters. Yoshii and Okazaki [13] have performed molecular-dynamics studies of cluster structure in a Lennard-Jones fluid which is just above its critical temperature. They used 10 976 atoms with a force cutoff of 4.9σ and defined the clusters based on the bond length of 1.24σ, as in our work. They examined the cluster structure at densities below the critical density, since above the critical density the clusters tend to be connected throughout the periodic domain. The components of the inertia tensor are given by terms like $I_{xy}=\Sigma(x_i-x_{\rm cm})(y_i-y_{\rm cm})$, where the summation is over the n atoms in the cluster, which has a center of mass at $(x_{\rm cm},y_{\rm cm},z_{\rm cm})$. The radius of gyration R_g is the square root of the mean-square average distance from the center of mass, $R_g=\sqrt{(I_{xx}+I_{yy}+I_{zz})/n}$. Yoshii and Okazaki present the radius of gyration as a function of cluster size and find that it has a fractal character. Using the relation $R_g^{D_f}=n$, where n is the cluster size and D_f is the fractal dimension determined from a log-log plot of radius versus cluster size, they obtain a value of 2.25 (earlier work by Heyes and Melrose reports a value of 2.35 ± 0.1 [14]). We find a range of values: from an exponent of 3.0 when $\eta=0.125$ to a value of 2.15 when $\eta=2$. Hence the fractal nature of our clusters depends upon the rate at which they have formed. Figure 12 presents the radius of gyration in the case of η equal to 0.5. The line indicates that $D_f=2.5$; when the expansion rate is unity, $D_f=2.25$ (not shown, but similar to the results of Yoshii and Okazaki, except that our cluster-size range is much smaller).

The changing fractal nature with expansion rate also affects the distributions of cluster size. The cumulative cluster distributions, which are used to determine the mean cluster size, have been based on cluster mass, that is, the number of

atoms. At low expansion rates in the MD simulations, a distribution based on cluster diameter (cube root of mass) appears to provide the same mean cluster size as those based on mass, but, when the expansion rate is larger than 0.25, then the diameter-based distribution does not have any constant slope region from which a mean size can be selected. A discussion of mass- versus diameter-based distributions is given by Holian and Grady [1] and by Grady and Kipp [15].

Further information about the cluster shape can be found by examining the shape of the inertia tensor. We form the complete inertia tensor and then diagonalize the matrix to obtain the eigenvalues. The eigenvalues are arranged in the order $a \geq b \geq c$; the radius of gyration equals $\sqrt{a^2+b^2+c^2}$. A rodlike object will have $a > b,c$ and a pancake shape has $a,b > c$. We have formed the ratios b/a and c/a; the first ratio can be in the range from zero to unity and the second ratio from zero to the value of the first ratio. At $\eta = 0.5$, the average values of these ratios are $b/a \sim 0.7$, $c/a \sim 0.5$; at $\eta = 0.125$ both ratios have larger values: ~ 0.8 and ~ 0.6. Thus, at low expansion rate, the clusters exhibit more of a spherical character in comparison to the shapes produced by large expansion rates, where the maximum moment is more than twice the minimum inertia moment.

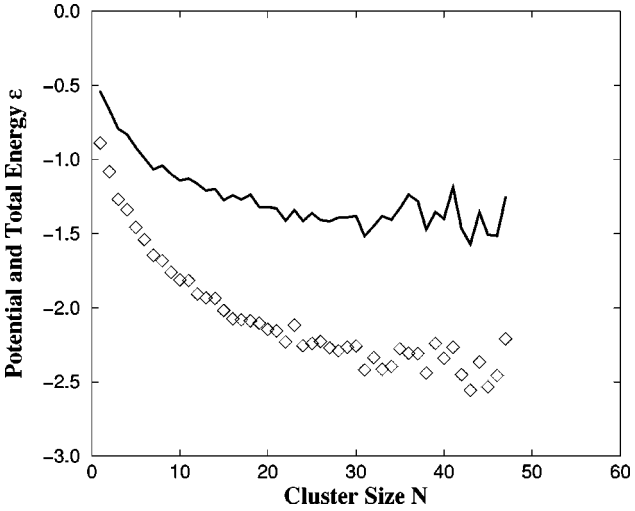

FIG. 13. The average cluster potential ($\diamond$) and total energy (solid line) indicate that almost all clusters have a negative total energy, and thus are likely to remain as a cluster; results from 32 K system size in 3D with an expansion rate $\eta = 0.5$. Here the largest clusters have about half of the initial liquid state potential energy, which is equal to -4.5.

APPENDIX C: CLUSTER BONDING

The clusters are defined by the bonds between atoms which have a smaller separation distance than the inflection point of the Lennard-Jones potential, 1.24σ. Yoshii and Okazaki [13] find that within a cluster each atom has on average a low number of these cluster-defining bonds; about three-fourths of the atoms have three or fewer of these bonds. In our clusters we find similar behavior, but notice that these bonds account for less than half of the atom potential energy. When we examine all bonds of the atoms within a cluster (separations up to the distance of the force cutoff, 2.5σ), we find that the number of bonds approaches the number of atoms in the small clusters (the maximum number of bonds is about 60 at low expansion rate and 18 at large expansion while over this same expansion range the maximum number of the cluster-defining bonds changes from 12 to 7). When we compare the energy given by all the bonds of an atom (giving half of the potential energy to each atom forming the bond) with just those bonds defined by atoms within the same cluster, we obtain an energy difference of only a few percent. Thus, most of the potential binding energy is between the atoms within the defined cluster; this would be the intracluster potential energy. Adding the atomic kinetic energy (with respect to the cluster center-of-mass velocity) to the intracluster potential energy, we find that almost all clusters have a total energy less than zero (see Fig. 13). At $\eta = 0.5$, the clusters which have only three or four atoms have less than 1% of their population with total energy greater than zero (remember the clusters are defined only by their geometry at the instant of inspection, and those few clusters with positive energy may represent a collision between a monomer and a smaller cluster, and thus at earlier and later times they may not be counted as the same cluster). At the low expansion rate of 0.05 and the cluster size of three, there are 7% of the clusters with positive energy; the rest of the clusters have negative total energy. And at these low expansion rates, the very large clusters have a potential energy value close to the initial liquid state value, implying that the cluster density is approximately the initial triple point density.

Figure 14 presents distributions of the number of bonds in small clusters formed at large expansion rates and in large clusters formed at small expansion rates. In accumulating the bonds of each atom, only those with a length of less than 1.61σ were considered (this gives a bond energy less than -0.2ϵ and provides most of the atom potential energy when all bond lengths out to a distance of 2.5σ are considered). The dashed line is the histogram of the number of bonds found in 28 clusters created by $\eta = 0.5$ (there are a total of

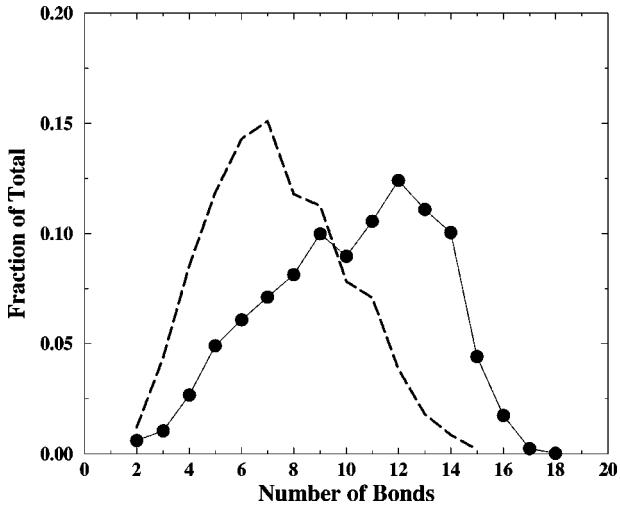

FIG. 14. Probability of the number of bonds in a 3D cluster. In large clusters ($\eta = 0.125$, cluster size from 500 to 710, filled circles) the most probable number of bonds (12) is equal to the number of nearest neighbors in the liquid state while in small clusters ($\eta = 0.5$, cluster size from 50 to 72, dashed line) the most likely number of bonds is only seven; results from 32 K system size.

1510 atoms in the examined clusters). These clusters represent the largest cluster size formed at this expansion rate, and their most likely number of bonds is about half that of the initial liquid state value, 7 compared to 12, and only 22% of the atoms have more than nine bonds. At low expansion rate, $\eta = 0.125$ (filled circles), the most probable number is the same as the number of nearest neighbors in the liquid state with 30% of the atoms having fewer than nine bonds (there are nine clusters in this sample with a total of 5175 atoms). One reason for the shift in these distributions is the change in the fraction of atoms which are surface atoms with the change in spherical volume. Packing spheres with diameter σ into a volume with radius R results in the fraction of surface atoms being equal to $3\sigma/2R$. The largest cluster in Fig. 11 has a radius of about 5σ, which gives 30% of the atoms at the surface, and implies that these are the atoms with fewer than nine bonds. The other, smaller cluster in Fig. 11 is not spherical, but using a radius of 2σ as representative of its size, it leads to about 20% interior atoms (and those have more than nine bonds each).

[1] B. L. Holian and D. E. Grady, Phys. Rev. Lett. **60**, 1355 (1988).
[2] D. E. Grady, J. Appl. Phys. **53**, 322 (1982).
[3] S. Toxvaerd, Phys. Rev. E **58**, 704 (1998).
[4] J. A. Blink and W. G. Hoover, Phys. Rev. A **32**, 1027 (1985).
[5] L. Verlet, Phys. Rev. **159**, 98 (1967).
[6] B. Smit, J. Chem. Phys. **96**, 8639 (1992).
[7] J. K. Johnson, J. A. Zollweg, and K. E. Gubbins, Mol. Phys. **78**, 591 (1993).
[8] B. Smit and D. Frenkel, J. Chem. Phys. **94**, 5663 (1991).
[9] B. L. Holian and R. Ravelo, Phys. Rev. B **51**, 11 275 (1995).
[10] B. L. Holian, Phys. Rev. B **22**, 1394 (1980); M. Ross, Phys. Rev. **184**, 233 (1969).
[11] M. Mecke, J. Winkelmann, and J. Fischer, J. Chem. Phys. **107**, 9264 (1997).
[12] E. L. Knuth and U. Henne, J. Chem. Phys. **110**, 2664 (1999).
[13] N. Yoshii and S. Okazaki, J. Chem. Phys. **107**, 2020 (1997).
[14] D. M. Heyes and J. R. Melrose, Mol. Phys. **66**, 1057 (1989).
[15] D. E. Grady and M. E. Kipp, J. Appl. Phys. **58**, 1210 (1985).